INORGANIC CHEMISTRY

Side-on coordination of diphosphorus to a mononuclear iron center

Shuai Wang[1], Jeffrey D. Sears[2], Curtis E. Moore[3], Arnold L. Rheingold[1], Michael L. Neidig[2], Joshua S. Figueroa[1]*

The diagonal relationship in the periodic table between phosphorus and carbon has set an expectation that the triple-bonded diatomic diphosphorus molecule (P_2) should more closely mimic the attributes of acetylene (HC≡CH) rather than its group 15 congener dinitrogen (N_2). Although acetylene has well-documented coordination chemistry with mononuclear transition metals, coordination complexes that feature P_2 bound to a single metal center have remained elusive. We report the isolation and x-ray crystallographic characterization of a mononuclear iron complex featuring P_2 coordination in a side-on, η^2-binding mode. An analogous η^2-bound bis-timethylsilylacetylene iron complex is reported for comparison. Nuclear magnetic resonance, infrared, and Mössbauer spectroscopic analysis—in conjunction with density functional theory calculations—demonstrate that η^2-P_2 and η^2-acetylene ligands exert a similar electronic demand on mononuclear iron centers but exhibit different reactivity profiles.

In main group chemistry, the diagonal relationship between certain second- and third-period elements of the periodic table has long provided a conceptual framework for rationalizing anomalous trends in chemical reactivity (*1*, *2*). The reactivity and structural patterns of most elements are dictated by their valence shell electron configuration, which is conserved within a periodic group. However, for cases in which the diagonal relationship holds, trends in the chemical reactivity of one element can more closely parallel those of an element of an adjacent group and neighboring period, where electronegativity and frontier orbital energies find greater convergence (*2*). For molecular systems, an iconic diagonal relationship has long been recognized to exist between carbon and phosphorus, especially in cases where element-element multiple bonding is present (*3*). In the most fundamental manifestation of element-element multiple bonding, the chemical and electronic structural properties of the free, triple-bonded diphosphorus molecule (P_2) have been shown, both experimentally and theoretically, to more closely mimic those of acetylene (HC≡CH) rather than its group 15 congener dinitrogen (N_2) (*4*–*8*). Similar to triple-bonded acetylene, the reactivity of diphosphorus is dominated by high-energy π bonds, which lie above the corresponding σ-bonding interaction (Fig. 1A) (*6*, *7*). By contrast, the π-bonding interactions of dinitrogen fall below the energy of the σ-bond, which is inherently low in energy on account of the greater electronegativity of nitrogen relative to carbon and phosphorus (Fig. 1A) (*6*, *7*).

Despite this diagonal relationship, diphosphorus—unlike acetylene—is a highly unstable and reactive molecular species. When generated in free form, diphosphorus is a fleeting species that either rapidly polymerizes (*9*, *10*) or reacts with substrate molecules present in the medium through both π bonds (*5*, *11*–*13*). The origin of this instability lies in the relatively weak nature of the triple bond in diphosphorus [D_e(P≡P) = 117 kcal/mol; D_e represents the triple bond dissociation energy] (*14*), which is substantially weaker than that of acetylene [D_e(HC≡CH) = 230 kcal/mol] or dinitrogen [D_e(N≡N) = 226 kcal/mol] (*14*, *15*). Correspondingly, the gap between the highest occupied molecular orbital (HOMO) and lowest unoccupied molecular orbital (LUMO) of diphosphorus is substantially smaller than that of either N_2 or acetylene, thereby signifying a less stable molecular system (Fig. 1A). For decades, one successful strategy for stabilization of reactive π-bonded polyphosphorus species has been complexation to a single transition metal center (*16*). Indeed, cyclic polyphosphorus aromatic species that mimic the conjugated π systems of the cyclopropenium cation [i.e., (*cyclo*-C_3H_3)$^+$], cyclobutadiendiyl dianion [i.e., (*cyclo*-C_4H_4)$^{2-}$] and cyclopentadienyl monoanion [i.e., (*cyclo*-C_5H_5)$^-$] have all been isolated as adducts to a single metal center (Fig. 1B) (*16*). These cyclic polyphosphorus compounds are among the most prominent manifestations of the diagonal relationship between phosphorus and carbon and have been extensively studied in the context of aromaticity within inorganic systems (*17*, *18*). However, coordination compounds that feature the binding of P_2 to a single metal, where a P-P π bond remains intact and does not benefit from aromatic stabilization, have proved to be elusive targets (*11*, *19*). This is despite theoretical predictions that P_2 can bind effectively in a side-on configuration (*20*), analogous to acetylene and other alkynes, which have an extensive documented mononuclear coordination chemistry (*21*, *22*). In addition, phosphaalkynes (i.e., P≡CR, where R denotes an organic substituent)—which possess a direct P-C triple bond and also illustrate the carbon-phosphorus diagonal relationship—have long been established to bind mononuclear transition metals in a side-on configuration (*23*). Here, we provide synthetic, x-ray crystallographic, and spectroscopic details on an isolable mononuclear iron complex featuring a side-on–bound P_2 molecule. Key to the preparation of this compound is an alternative synthetic strategy that circumvents the intermediacy of free diphosphorus and allows for P-P multiple bond formation within a kinetically stabilizing steric environment.

Multiple synthetic routes have been established for the formation of multinuclear diphosphorus complexes (*24*–*27*). Most common among these is the reductive cleavage of the tetrahedral P_4 molecule (i.e., white phosphorus) by low-valent transition metal complexes or the photolytic fragmentation of P_4 in the presence of metal-based acceptor compounds (*24*, *25*). In such reactions, mononuclear P_2 complexes have been proposed as the key unobserved intermediates before aggregation (*28*). Over the past several years, well-defined reagents have been developed—most prominently by Cummins and colleagues (*11*, *12*)—to install P_2 units on transition metal centers by the release of diphosphorus equivalents in solution. In reactions using these reagents, mononuclear transition metal P_2 complexes have also been proposed as intermediates, but these rapidly dimerize or are intercepted by unsaturated organic substrates to furnish products in which both P-P π bonds are cleaved (*11*, *12*, *19*). A less common method for generating multinuclear P_2 complexes is the reaction between a metal-based nucleophile and common phosphorus-based electrophiles. This was the procedure employed by Markó and colleagues in 1973 to produce the first multinuclear P_2 complex, (μ_2-η^2:η^2-P_2)$Co_2(CO)_6$, from the nucleophilic carbonylmetallate salt Na[$Co(CO)_4$] and PCl_3 (*29*). However, the infrequent application of this metal-nucleophile and phosphorus-electrophile route stems from the ill-defined nature of the P-P bond formation step. We hypothesized that P-P bond formation in this system may occur by direct electrophilic attack by PCl_3 on metal organophosphide intermediates (i.e., M-PCl_2). Moreover, we reasoned that this strategy could provide a mononuclear P_2 complex if a protective coordination platform was employed in conjunction with kinetically labile leaving groups on the phosphorus atoms. Accordingly, we targeted the reaction between the meta-terphenyl isocyanide complex, $K_2[Fe(CO)_2(CNAr^{Dipp2})_2]$ (K_2[**1**];

[1]Department of Chemistry and Biochemistry, University of California, San Diego, 9500 Gilman Drive, Mail Code 0358, La Jolla, CA, 92093-0358, USA. [2]Department of Chemistry, University of Rochester, Rochester, NY 14627, USA. [3]Department of Chemistry, The Ohio State University, 88 West 18th Avenue, Columbus, OH 43210, USA.
*Corresponding author. Email: jsfig@ucsd.edu

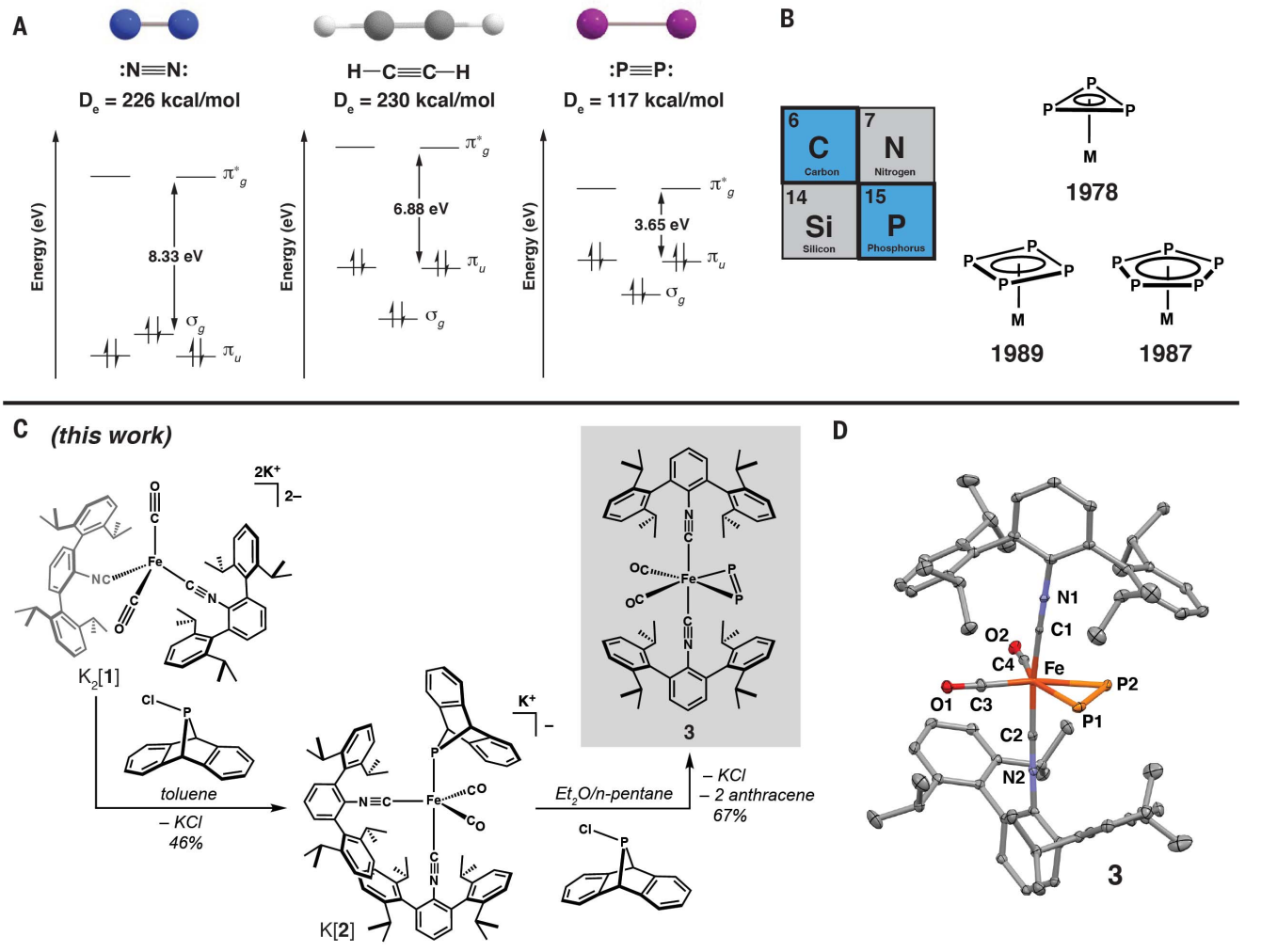

Fig. 1. The diagonal relationship between phosphorus and carbon. (**A**) Partial molecular orbital diagrams for dinitrogen (N_2), acetylene (HC≡CH), and diphosphorus (P_2) showing the relative energetic ordering of the frontier σ- and π-symmetry orbitals of the triple bonds. Molecular orbital energy gaps are derived from density functional theory calculations at the BP86/def2-TZVP level. (**B**) Schematic representation and date of discovery of transition-metal (M)–bound polyphosphorus aromatic ligands that mimic carbon-based cyclic aromatic molecular species according to the diagonal relationship between phosphorus and carbon. (**C**) Schematic representation of the synthetic route to the mononuclear iron η^2-diphosphorus complex **3**. Et, ethyl, CH_2CH_3. (**D**) X-ray crystal structure of the mononuclear iron η^2-diphosphorus complex **3**. Hydrogen atoms have been omitted for clarity.

Ar^{Dipp2} = 2,6-(2,6(*i*-Pr)$_2$C$_6$H$_3$)$_2$C$_6$H$_3$; *i*-Pr = iso-propyl; Fig. 1C (*30*) and the anthracendiyl-substituted chlorophosphine, ClP(anth) (anth = 9,10-anthracendiyl; Fig. 1C). Complex K_2[**1**] features a nucleophilic Fe(–II) center in a sterically encumbered environment, whereas the electrophilic ClP(anth) scaffold is highly susceptible to carbon-phosphorus bond homolysis under mild conditions and can therefore serve as a source of phosphorus atoms for diphosphorus formation (*31*).

Addition of 1.0 equivalents of ClP(anth) to K_2[**1**] in cold toluene solution (–100°C) proceeds with the loss of 1.0 equivalent of potassium chloride (KCl) to yield the salt K[Fe(P(anth))(CO)$_2$($CNAr^{Dipp2}$)$_2$] (K[**2**]; Fig. 1C], which contains an intact anthracendiyl-substituted phosphanyl ligand as determined by single-crystal x-ray diffraction (fig. S15). Complex K[**2**] persists at room temperature in benzene-d_6 solution for up to 5 days without noticeable decomposition. However, when K[**2**] is treated with a second equivalent of ClP(anth) in a 3:1 diethyl ether/*n*-pentane mixture at low temperature (–100°C; Fig. 1C), the rapid precipitation of a bright yellow solid is observed. Extraction of this solid into toluene, followed by crystallization at –40°C and structural analysis by means of x-ray crystallography, revealed it to be the mononuclear, side-on–bound diphosphorus complex (η^2-P$_2$)Fe(CO)$_2$($CNAr^{Dipp2}$)$_2$ (**3**; Fig. 1D), thereby demonstrating that the diatomic P_2 molecule can be constructed by successive electrophilic additions to a metal-based nucleophile.

To understand the mechanistic steps leading to P-P bond formation in this system, K[**2**] was treated with the diorganochlorophosphines $ClPPh_2$ (Ph, phenyl, C_6H_5) and ClP(*i*-Pr)$_2$, both of which are phosphorus-based electrophiles that do not readily undergo P-C bond homolysis. These reactions proceeded cleanly at –100°C in diethyl ether solution to eliminate KCl and produce, as determined by x-ray crystallography, the neutral phosphanylphosphine complexes Fe(κ^1-P(anth)PPh_2)(CO)$_2$($CNAr^{Dipp2}$)$_2$ (**4**^{PPh2}) and Fe(κ^1-P(anth)P(*i*-Pr)$_2$)(CO)$_2$($CNAr^{Dipp2}$)$_2$ (**4**$^{P(i\text{-}Pr)2}$), in which new P-P single bonds are established (Fig. 2A). Presumably, the encumbering steric environment of complex K[**2**] disfavors reaction products where a second electrophilic substrate is directly added to the iron center. However, complexes **4**^{PPh2} and **4**$^{P(i\text{-}Pr)2}$ are both thermally stable at room temperature in benzene-d_6 solution as intermittently assayed

by ^{1}H nuclear magnetic resonance (NMR) spectroscopy over the course of 3 days. Accordingly, a reasonable mechanistic pathway to the mononuclear diphosphorus complex ***3*** is through the putative intermediate Fe(κ^1-P(anth)P(anth))$(CO)_2$$(CNAr^{Dipp2})_2$ ($\mathbf{4}^{P(anth)}$-Int; Fig. 2B), containing a κ^1-bound phosphanylphosphine ligand with two anthracendiyl substituents. Anthracene extrusion from the distal P(anth) group relative to the iron center in $\mathbf{4}^{P(anth)}$-Int can then afford the phosphanylphosphinidene intermediate (*32*), Fe(η^2-(P≡P(anth)))$(CO)_2$$(CNAr^{Dipp2})_2$ (***5***-Int; Fig. 2B), from which loss of a second equivalent of anthracene generates the diphosphorus ligand. In support of this mechanistic scenario is the isolation of the borane-substituted phosphine complex Fe(κ^1-P(anth)B(9-BBN))$(CO)_2$$(CNAr^{Dipp2})_2$ ($\mathbf{4}^{BBN}$; Fig. 1A), through the reaction between K[***2***] and iodo-9-BBN (9-BBN = 9-borabicyclo[3.3.1]nonane). The 9-BBN fragment has a steric profile similar to that of a P(anthracendiyl) unit but is not known to undergo carbon-boron bond homolysis under ambient conditions. Most notably, complex $\mathbf{4}^{BBN}$ is also thermally stable at room temperature for at least 3 days in benzene-d_6 solution. This thermal stability strongly indicates that ejection of the distal anthracendiyl unit in $\mathbf{4}^{P(anth)}$-Int is a crucial step leading to diphosphorus complex ***3*** after initial P-P bond-formation through nucleophile-electrophile coupling.

The solid-state molecular structure and spectroscopic signatures of complex ***3*** are consistent with its formulation as a mononuclear diphosphorus complex possessing phosphorus-phosphorus multiple bonding interactions. Inspection of the solid-state packing diagram for ***3*** reveals that each (η^2-P_2)Fe-containing molecule is a discrete monomeric species, with the closest distance between the P_2 units and any neighboring iron center being 10.6(3) Å (fig. S18; number in parentheses represents estimated standard deviation). Complex ***3*** crystallizes with two crystallographically independent molecules in the unit cell, which give rise to statistically indistinguishable P-P bond distances of 1.987(3) Å and 1.989(3) Å. The average P-P bond distance for ***3*** [1.988(1) Å] is elongated relative to that experimentally determined for free P_2 [d(P-P) = 1.8934 Å] (*14*). However, it is shorter than the average P=P double bond distance of structurally characterized organodiphosphene compounds [i.e., RP=PR; d(P-P) = 2.035(±0.018) Å] as well as the average P-P bond distance in structurally characterized, dinuclear transition-metal diphosphorus complexes [i.e., (μ_2-P_2)M_2 and (μ_2-η^2:η^2-P_2)M_2; d(P-P) = 2.103(±0.045) Å] (*33*). It is also substantially contracted relative to the P-P single bond distance in the tetrahedral P_4 molecule [*d*(P-P) = 2.21(1) Å] (*34*). Accordingly, these latter comparisons reflect that

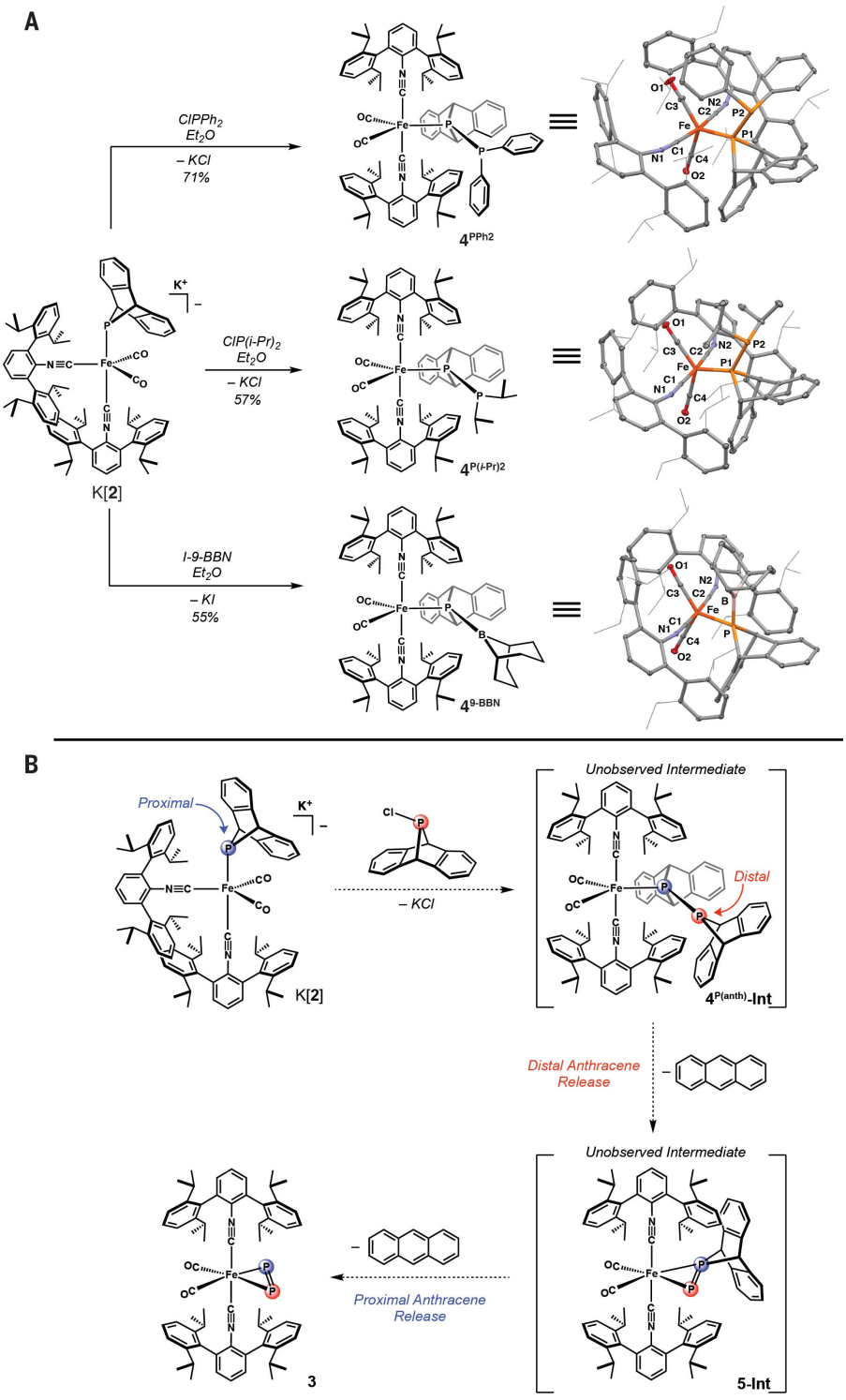

Fig. 2. Mechanistic interrogation of diphosphorus formation on a mononuclear iron center. (**A**) Schematic representation of the synthetic route to the heteroatom-substituted phosphine complexes $\mathbf{4}^{PPh2}$, $\mathbf{4}^{P(i\text{-}Pr)2}$ and $\mathbf{4}^{BBN}$, which demonstrate that the phosphorus atom in the 9,10-anthracendiylphosphanyl salt K[**2**] serves as the ultimate site of electrophilic addition. X-ray crystallographic structures of $\mathbf{4}^{PPh2}$, $\mathbf{4}^{P(i\text{-}Pr)2}$, and $\mathbf{4}^{BBN}$ are shown to the right. For all structures, the iso-propyl groups of the $CNAr^{Dipp2}$ ligands are depicted as wireframe for clarity. (**B**) Proposed mechanism for the formation of the mononuclear η^2-P_2 complex **3** through the intermediacy of the unobserved species $\mathbf{4}^{P(anth)}$-Int and **5**-Int. Initial anthracene release from the distal position in the phosphanyl-phosphine intermediate $\mathbf{4}^{P(anth)}$-Int is proposed to provide the 9,10-anthracendiyl phosphanylphosphinidene intermediate **5**-Int. Anthracene release from **5**-Int provides mononuclear η^2-P_2 complex **3**.

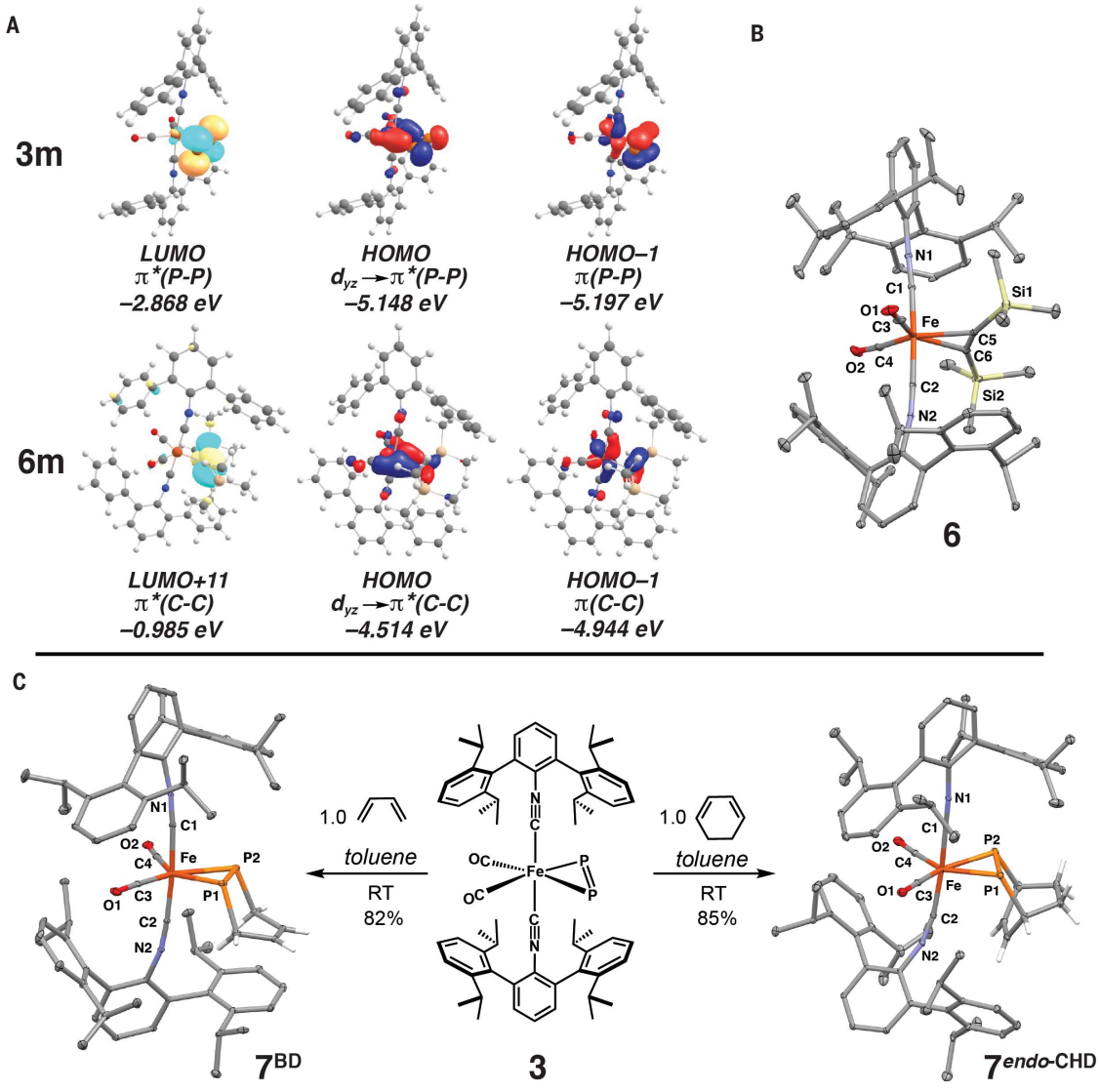

Fig. 3. Electronic structure and reactivity of mononuclear η^2-acetylene and η^2-diphosphorus complexes. (**A**) Density functional theory–calculated molecular orbitals for the model complexes **3m** and **6m** comparing the electronic structure attributes of the π/π^* orbital manifold of the η^2-P_2 and η^2-bis-trimethylsilylacetylene (BTMSA) ligands, respectively. (**B**) X-ray crystal structure of the mononuclear iron BTMSA complex **6**. Hydrogen atoms have been omitted for clarity. (**C**) Reactivity of complex **3** with 1,3-butadiene (BD) and 1,3-cyclohexadiene (CHD) to generate the diphospha-Diels-Alder adducts $\mathbf{7}^{BD}$ and $\mathbf{7}^{endo\text{-}CHD}$ as represented by x-ray crystallographic structures. The hydrogen atoms of the cyclic diphosphene ligands in the structures of $\mathbf{7}^{BD}$ and $\mathbf{7}^{endo\text{-}CHD}$ have been included to indicate the regiochemical outcome of the diphospha-Diels-Alder reaction. All other hydrogen atoms have been omitted for clarity. RT, room temperature.

considerable phosphorus-phosphorus multiple bonding is retained upon coordination of the P_2 to a single iron center. Moreover, the ^{31}P NMR spectroscopic features of **3** are also consistent with the presence of multiple bonding character. In benzene-d_6 solution, **3** gives rise to a single downfield resonance centered at δ = 434.4 parts per million (ppm; δ, chemical shift) (fig. S6), which is within the range expected for electronically unsaturated phosphorus nuclei. The ^{31}P NMR chemical shift of complex **3** can be further compared to those measured experimentally for P_4 (δ = –540 ppm) (*35*) and calculated for free P_2 by means of density functional theory (δ = 689.3 ± 45.4 ppm) (*36*–*38*). Although the ^{31}P NMR chemical shift of **3** more closely matches free P_2 rather than the electronically saturated P_4 molecule, the greater shielding of the resonance exhibited by **3** relative to free P_2 is indicative of an increased energetic separation between the magnetically coupled phosphorus-based π-bonding and π*-antibonding orbitals upon coordination to a single metal center. Accordingly, this spectroscopic feature of the (η^2-P_2)Fe interaction in **3** is consistent with the Dewar-Chatt-Duncanson bonding model (*39*), wherein σ-donation from the P_2 ligand to iron energetically stabilizes one P-P π bond, whereas π backdonation from iron results in energetic destabilization of the P-P π* molecular orbital relative to that found in free P_2.

Density functional theory calculations provide additional support for the presence of iron-to-P_2 π-backdonation in complex **3**, as well as retention of P-P π bonding. Analysis of the molecular orbitals calculated for the model complex (η^2-P_2)$Fe(CO)_2(CNAr^{Ph2})_2$ (**3m**; Ar^{Ph2} = 2,6-$(C_6H_5)_2C_6H_3$) revealed a HOMO consistent with a π-backbonding interaction from iron to the η^2-P_2 unit in the direction perpendicular to the axially-disposed isocyanide

ligands (Fig. 3A). Correspondingly, the calculated HOMO-1 comprised an unperturbed P-P π bond in the direction parallel to the isocyanide ligands (Fig. 3A). Natural bond orbital (NBO) calculations on **3m** resulted in a Wiberg bond index (WBI) of 2.182 for the η^2-P_2 ligand. Although this value is less than that calculated for the canonical triple bond in free P_2 [3.000] (*20*), it indicates that the primary orbital interactions between iron and the η^2-P_2 in ***3*** involve only one P-P π bond. Vibrational frequency calculations on model **3m** also indicated that the π-bonding manifold of the η^2-P_2 ligand is weakened—but not eliminated—upon coordination to a single iron center. These calculations on **3m** predicted a low-intensity ν_{PP} stretching band of 668 cm^{-1} (fig. S27), which is red-shifted relative to that measured for free P_2 (ν_{PP} = 781 cm^{-1}) (*14*) and is in accord with electronic occupation of one P-P π* orbital through π-backdonation. Notably, the solid-state infrared spectrum of complex ***3*** features a low-intensity band centered at 674 cm^{-1} that is consistent with the ν_{PP} stretch calculated for **3m** (fig. S12). This assignment is further corroborated by comparison to the infrared spectrum of the tricarbonyl complex $Fe(CO)_3(CNAr^{Dipp2})_2$ (***5***), which presents a similar spectral fingerprint pattern as that of complex ***3***, but does not feature this low-intensity band (fig. S12).

To gain additional insight into the properties and electronic influence of the η^2-P_2 ligand in complex ***3***, the η^2-alkyne complex (η^2-BTMSA)$Fe(CO)_2(CNAr^{Dipp2})_2$ (**6**; BTMSA = bis-trimethylsilylacetylene) was prepared for comparison and characterized by x-ray crystallography (Fig. 3B). In the solid state, complex **6** is isostructural to ***3*** and features an η^2-*C,C* bound BTMSA ligand, consistent with the qualitative electronic analogy between alkynes and diphosphorus. However, Mössbauer spectroscopic measurements on complexes ***3*** and **6** revealed nearly identical isomer shifts (δ = 0.03 and 0.04 mms^{-1}, respectively), thereby providing a quantitative assessment that η^2-alkyne and η^2-P_2 ligands exert a similar electronic demand on a mononuclear iron center (figs. S13 and S14). By contrast, the Mössbauer quadrupole splitting parameters (ΔE_Q) for complexes ***3*** (0.97 mms^{-1}) and **6** (1.38 mms^{-1}) are dissimilar, which is attributed to electric-field effects originating from the noncoordinated, phosphorus-based lone pairs of the η^2-P_2 ligand of complex ***3***, as well as potential contributions from the larger covalent radius of phosphorus relative to carbon in the η^2-P_2 and η^2-BTMSA ligands, respectively (*40*).

Although P_2 and BTMSA exhibit similar binding properties to a mononuclear iron center, their reactivity profiles as coordinated ligands are substantially disparate. Analysis of the LUMO calculated for model **3m** revealed that it exclusively constitutes a P-P π* orbital in the direction perpendicular to the (η^2-P_2)Fe bonding vector (Fig. 3A). By contrast, the corresponding C-C π* orbital calculated for the model complex (η^2-*C,C*-BTMSA)$Fe(CO)_2(CNAr^{Ph2})_2$ (**6m**) is considerably higher in energy (LUMO +11; Fig. 3A), thereby suggesting that the electrophilic character of the alkyne ligand in **6** will be substantially diminished relative to the P_2 ligand in ***3***. Moreover, the quantitative energetic differences between the intact π-bonding and the corresponding π*-antibonding orbitals calculated for **3m** and **6m** parallel those for free P_2 and acetylene (Figs. 1A and 3A). Consistent with this notion is the finding that complex **6** fails to react with the diene nucleophiles 1,3-butadiene (BD) and 1,3-cyclohexadiene (CHD) at room temperature in toluene solution. However, complex ***3*** reacts readily with these substrates under identical conditions to yield the corresponding diphospha-Diels-Alder adducts $\mathbf{7}^{BD}$ and $\mathbf{7}^{endo\text{-}CHD}$, respectively, in which phosphorus-carbon single bonds are established (Fig. 3C). Crystallographic characterization of $\mathbf{7}^{BD}$ and $\mathbf{7}^{endo\text{-}CHD}$ confirmed that the diphosphorus units in these Diels-Alder adducts remain coordinated to the iron center and possess P-P bond distances [*d*(P-P = 2.123(1) Å and 2.1118(10) Å for $\mathbf{7}^{BD}$ and $\mathbf{7}^{endo\text{-}CHD}$, respectively] which are elongated relative to that in ***3*** in a manner consistent with cleavage of the remaining P-P π bond (Fig. 3C).

The diagonal relationship between phosphorus and carbon has long provided a conceptual expectation for the coordination chemistry of the triple-bonded diphosphorus molecule to be analogous to acetylene. The work presented here experimentally affirms this relationship and provides a synthetic strategy to access mononuclear complexes of diphosphorus in laboratory settings. It is anticipated that this coordination mode, in which the π-bonding framework of P_2 is partially maintained, may further enable the development of selective phosphorus-atom transfer reactions to organic molecules.

REFERENCES AND NOTES

1. N. N. Greenwood, A. Earnshaw, *Chemistry of the Elements* (Butterworth-Heinemann, ed. 2, 1997).
2. G. Rayner-Canham, *Found. Chem.* **13**, 121–129 (2011).
3. K. Dillon, F. Mathey, J. Nixon, *Phosphorus: The Carbon Copy: From Organophosphorus to Phospha-Organic Chemistry* (Wiley, 1998).
4. N. A. Piro, C. C. Cummins, *J. Am. Chem. Soc.* **130**, 9524–9535 (2008).
5. D. Tofan, C. C. Cummins, *Angew. Chem. Int. Ed.* **49**, 7516–7518 (2010).
6. K. I. Goldberg, D. M. Hoffman, R. Hoffmann, *Inorg. Chem.* **21**, 3863–3868 (1982).
7. W. Kutzelnigg, *Angew. Chem. Int. Ed.* **23**, 272–295 (1984).
8. L. T. Xu, T. H. Dunning Jr., *J. Chem. Theory Comput.* **11**, 2496–2507 (2015).
9. H. W. Melville, S. C. Gray, *Trans. Faraday Soc.* **32**, 271–285 (1936).
10. D. P. Stevenson, D. M. Yost, *J. Chem. Phys.* **9**, 403–408 (1941).
11. N. A. Piro, J. S. Figueroa, J. T. McKellar, C. C. Cummins, *Science* **313**, 1276–1279 (2006).
12. A. Velian *et al.*, *J. Am. Chem. Soc.* **136**, 13586–13589 (2014).
13. D. Rottschäfer *et al.*, *Chemistry* **25**, 8127–8134 (2019).
14. K. P. Huber, G. Herzberg, *Constants of Diatomic Molecules*, vol. IV of *Molecular Spectra and Molecular Structure* (Van Nostrand Reinhold, 1979).
15. S. W. Benson, *J. Chem. Educ.* **42**, 502 (1965).
16. E. Peresypkina, A. Virovets, M. Scheer, *Coord. Chem. Rev.* **446**, 213995 (2021).
17. I. A. Popov, A. I. Boldyrev, in *The Chemical Bond*, G. Frenking, S. Shaik, Eds. (Elsevier, 2014), pp. 421–444.
18. F. Kraus, J. C. Aschenbrenner, N. Korber, *Angew. Chem. Int. Ed.* **42**, 4030–4033 (2003).
19. A. Velian, C. C. Cummins, *Chem. Sci.* **3**, 1003–1006 (2012).
20. C. Esterhuysen, G. Frenking, *Chemistry* **9**, 3518–3529 (2003).
21. J. Chatt, G. A. Rowe, A. A. Williams, *Proc. Chem. Soc.* 208 (1957).
22. J. L. Templeton, in *Advances in Organometallic Chemistry*, F. G. A. Stone, R. West, Eds. (Academic Press, 1989), vol. 29, pp. 1–100.
23. J. F. Nixon, *Coord. Chem. Rev.* **145**, 201–258 (1995).
24. B. M. Cossairt, N. A. Piro, C. C. Cummins, *Chem. Rev.* **110**, 4164–4177 (2010).
25. M. Caporali, L. Gonsalvi, A. Rossin, M. Peruzzini, *Chem. Rev.* **110**, 4178–4235 (2010).
26. L. Liu *et al.*, *Chem. Sci.* **7**, 2335–2341 (2016).
27. J. Sun *et al.*, *Chem* **7**, 1952–1962 (2021).
28. M. E. Barr, B. R. Adams, R. R. Weller, L. F. Dahl, *J. Am. Chem. Soc.* **113**, 3052–3060 (1991).
29. A. Vizi-Orosz, G. Pályi, L. Markó, *J. Organomet. Chem.* **60**, C25–C26 (1973).
30. A. E. Carpenter *et al.*, *Inorg. Chem.* **54**, 2936–2944 (2015).
31. W. J. Transue *et al.*, *J. Am. Chem. Soc.* **139**, 10822–10831 (2017).
32. J. Olkowska-Oetzel, J. Pikies, *Appl. Organomet. Chem.* **17**, 28–35 (2003).
33. C. S. Database, (CSD), version 2021.2 (Cambridge Crystallographic Data Center, 2021).
34. L. R. Maxwell, S. B. Hendricks, V. M. Mosley, *J. Chem. Phys.* **3**, 699–709 (1935).
35. K. A. Mandla, C. E. Moore, A. L. Rheingold, J. S. Figueroa, *Angew. Chem. Int. Ed.* **58**, 1779–1783 (2019).
36. P. Lazzeretti, J. A. Tossell, *J. Phys. Chem.* **91**, 800–804 (1987).
37. A. Dransfeld, D. B. Chesnut, *Chem. Phys.* **234**, 69–78 (1998).
38. A. Antušek, M. Jaszuński, M. Olejniczak, *Comput. Theor. Chem.* **970**, 54–60 (2011).
39. J. Chatt, L. A. Duncanson, *J. Chem. Soc.* 2939–2947 (1953).
40. P. Gütlich, E. Bill, A. X. Trautwein, *Mössbauer Spectroscopy and Transition Metal Chemistry: Fundamentals and Applications* (Springer, 2011).

ACKNOWLEDGMENTS

Funding: This work was supported by the US National Science Foundation through grants CHE-1802646 (to J.S.F.) and CHE-1954480 (to M.L.N.), as well as the US National Institutes of Health through grant R01GM111480 (to M.L.N.). **Author contributions:** S.W. carried out the synthetic work, analytical characterization, and computational studies. J.D.S. and M.L.N. performed the Mössbauer spectroscopy studies. S.W., C.E.M., and A.L.R. carried out the crystallographic studies. J.S.F. assisted with data analysis and directed the research. S.W. and J.S.F. wrote the manuscript, with input from all authors. **Competing interests:** The authors declare no competing interests. **Data and materials availability:** Crystallographic data for compounds K[**2**], **3**, $\mathbf{4}^{PPh2}$, $\mathbf{4}^{P(i\text{-}Pr)2}$, $\mathbf{4}^{BBN}$, **5**, **6**, $\mathbf{7}^{BD}$, and $\mathbf{7}^{endo\text{-}CHD}$ are available free of charge from the Cambridge Crystallographic Data Centre under references CCDC-2103243, CCDC-2103244, CCDC-2103245, CCDC-2103246, CCDC-2103247, CCDC-2103248, CCDC-2103249, CCDC-2103250, and CCDC-2103251, respectively. Additional spectroscopic, crystallographic, and computational data are included in the supplementary materials.

SUPPLEMENTARY MATERIALS

science.org/doi/10.1126/science.abn7100
Materials and Methods
Figs. S1 to S30
Tables S1 to S6
References (*41*–*61*)

14 December 2021; accepted 23 February 2022
10.1126/science.abn7100

Side-on coordination of diphosphorus to a mononuclear iron center

Shuai WangJeffrey D. SearsCurtis E. MooreArnold L. RheingoldMichael L. NeidigJoshua S. Figueroa

Science, 375 (6587), • DOI: 10.1126/science.abn7100

Sideways diphosphorus

Elemental phosphorus tends to form single-bonded clusters, in contrast to the triple-bonded diatomic of its periodic tablemate, nitrogen. It is nonetheless possible to synthesize and trap diphosphorus in certain circumstances, and S. Wang *et al*. now report a complex in which this species coordinates sideways to an iron center. The metal-ligand bonding motif, which was analyzed crystallographically, spectroscopically, and computationally, resembles coordination by triple-bonded carbons in alkynes. This similarity highlights the diagonal relationship between phosphorus and carbon in the periodic table. —JSY